

INFLUENCE OF THE FINITE LENGTH EFFECT ON THERMAL CREEP FLOW IN RAREFIED GAS

DOBRI Y. DANKOV^{*},

MIRONA K. MIRONOVA, PETER N. GOSPODINOV

Institute of Mechanics, Bulgarian Academy of Sciences

[Received: 17 September 2025. Accepted: 6 March 2026]

doi: <https://doi.org/10.55787/jtams.2026.1.AI00238>

ABSTRACT: This study analyzes the influence of finite-length effects on thermally induced flow in a rarefied monatomic gas between two stationary coaxial cylinders. Using the Direct Simulation Monte Carlo method, thermoacoustic waves induced by a sudden inner-cylinder temperature shock are examined under four axial boundary conditions: diffuse, adiabatic, symmetric, and periodic. Results reveal a transient regime, where thermoacoustic waves propagate and reflect depending on boundary type, and a steady-state regime, where temperature, density, and velocity profiles stabilize. Axial boundaries significantly affect wave dynamics, dissipation, and flow structure, particularly at intermediate and radial positions. The findings emphasize the importance of accurate boundary modeling in rarefied gas dynamics for applications in microscale devices, vacuum systems, and aerospace technologies.

KEY WORDS: Thermal creek flow, Rarefied gas, DSMC.

1 INTRODUCTION

In recent decades, the study of rarefied gas dynamics has gained increasing importance, driven by advancements in micro and nanoscale technologies, aerospace engineering, and high-vacuum systems. In rarefied regimes – characterized by Knudsen number (Kn), where the mean free path of gas molecules is not negligible relative to the system's geometric scale – the assumptions underpinning classical continuum fluid mechanics, such as the no-slip velocity condition and Fourier's law of heat conduction, cease to be valid. Instead, the interaction between gas molecules and bounding surfaces becomes a dominant factor in determining the macroscopic flow behavior. As such, the choice of boundary conditions plays a critical role in the accurate modeling and simulation of rarefied gas flows.

Unlike continuum flows, where boundaries are often treated as mathematically ideal surfaces with specified temperature or velocity, rarefied gas flows require boundary conditions that account for molecular-level physics. The Boltzmann equation and

^{*}Corresponding author e-mail: dankov@imbm.bas.bg

its reduced-order models (e.g., the BGK model, ES-BGK, and Shakhov models) describe gas dynamics in these regimes, and their solution demands the incorporation of appropriate gas-surface interaction models. These include diffuse reflection, where gas molecules are re-emitted from a wall with velocities sampled from a Maxwellian distribution based on wall conditions, and specular reflection, where molecules reflect without energy or momentum exchange. The degree of accommodation, often characterized by the momentum and energy accommodation coefficients, defines how closely real wall behavior aligns with these idealized models.

Additionally, thermal boundary conditions such as adiabatic walls (where no heat flux occurs) and isothermal walls (where temperature is held constant) are crucial in defining energy exchange at surfaces. For numerical modeling, periodic boundary conditions are commonly employed in simulations to mimic infinitely repeating domains, while symmetric conditions reduce computational effort by exploiting flow symmetries. Each of these conditions introduces distinct physical effects and numerical considerations, particularly in transitional and slip flow regimes.

The influence of boundary conditions extends beyond local wall phenomena, affecting global flow properties such as pressure distribution, mass flux, heat transfer rates, and flow stability. For example, in the context of microfluidic devices, boundary-driven rarefaction effects such as thermal creep, thermal transpiration, and velocity slip emerge directly from the imposed wall conditions. The cylindrical Couette flow of a rarefied gas between a rotating inner cylinder and a stationary outer cylinder is studied under two kinds of kinetic boundary conditions: one is the modified Maxwell-type boundary condition proposed by Dadzie and Méolans, and the other is the Cercignani-Lampis condition studied in [1]. As a result, the authors derive the condition for velocity slip and temperature jump corresponding to the above kinetic boundary conditions, which are necessary for the fluid-dynamic description of the small Knudsen number problem. In [2] is studied a temperature jump condition that includes the sliding friction. The temperature jump condition is evaluated for the NACA0012 micro-airfoil in high-speed rarefied gas flow simulations using the CFD method, which solves the Navier-Stokes equations within the OpenFOAM framework with working gas as air. In [3], the authors proposed a higher-order boundary condition based on Maxwell's general equation and the constitutive relations derived by Burnett. They show that these "Maxwell-Burnett" boundary conditions are in reasonable agreement with the limited experimental data available for Poiseuille flow and can also predict Sone's thermal-stress slip flow – a phenomenon that cannot be captured by conventional slip boundary conditions. In [4], the authors provide an analytical expression for the first- and second-order thermal slip coefficients by means of a vibrational technique that applies to the integrodifferential form of the Boltzmann equation based on the true linearized collision operator for hard-sphere

molecules. The Cercignani-Lampis scattering kernel of the gas-surface interaction has been considered in order to take into account the influence of the accommodation coefficients on the slip parameters. The conclusion in the work is that both accommodation coefficients increase by increasing the molecular weight of the considered gases. The oscillatory Stokes and the oscillatory Couette flows, as representative ones for harmonically oscillating half-space and finite-medium flow setups, respectively, are studied in [5]. The boundary conditions of the “positive” and “negative” moment equations are accordingly constructed from the half-range moments of the boundary conditions of the outgoing distribution function. Models of boundary conditions on the surface of a body for rarefied molecular gas taking into account the rotational energy are studied in [6]. A comparison of the temperature fields for the case of the flow past bodies is performed by the supersonic flow of a gas at incomplete energy accommodation on the surface and at various degrees of exchange of the rotational and translational energies. Authors in [7] kept the particle velocity magnitude invariant and the velocity direction of the reflected particle set based on isotropic scattering boundary conditions in the half space. The collision rule in [8] was applied everywhere on the wall with the normal velocity reversal, but with the two velocity components tangential to the wall, reflecting randomly. This treatment is a hybrid from one side with partial specular and from the other side diffuse reflection boundary conditions. In the real world, the normal velocity reversal is not always true. Rarefied gas flows induced by oscillating boundaries have attracted significant attention due to their applications in microscale pumping and acoustic flow control. In particular, Kosyanchuk conducted a numerical study of a microscale gas pump driven by surface acoustic waves, demonstrating that oscillatory wall motion can effectively generate directed gas flow under rarefied conditions [9]. The present work differs from that study in both geometry (cylindrical configuration vs. planar microchannel) and focus: here we investigate the influence of transverse boundary conditions on the flow structure rather than the pumping efficiency. Nevertheless, both studies highlight the importance of boundary-induced motion in controlling gas transport in rarefied regimes.

In our previous studies [10], we considered rarefied monatomic gas between two coaxial stationary cylinders (two dimensional axis-symmetrical problem) with a constant walls temperature, as the temperature profile of the wall of the inner cylinder (fiber) is stepwise. In [11], we study a rarefied monatomic gas between two coaxial, stationary, unconfined cylinders (one dimensional, axis-symmetrical problem). The temperature of the outer cylinder is constant and equal to the gas equilibrium while the temperature of the inner cylinder varies in time. The inner cylinder (filament) is subjected to a periodic heating-cooling cycle, which is modelled with diffuse and adiabatic boundary conditions. We previously studied the behavior of a rarefied gas

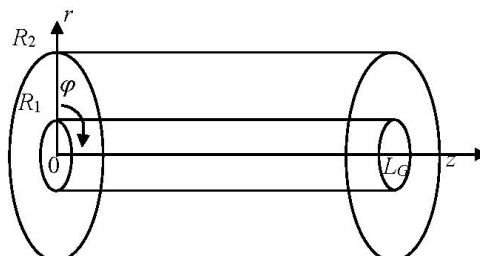


Fig. 1. The flow geometry.

between stationary cylinders subjected to oscillating and spatially nonuniform inner-wall temperature [12]. In that work, periodic boundary conditions were imposed on the cylinder cross sections.

The present study extends this analysis by examining the effect of different transverse boundary conditions on the resulting flow and temperature fields by using Direct Simulation Monte Carlo method. The hard-sphere (HS) molecular model was used to represent intermolecular collisions in the DSMC simulations. This choice is supported by our previous study [10–12], in which the DSMC results obtained with the HS model were compared to a direct numerical solution of the Navier–Stokes–Fourier equations, showing good agreement for both flow and thermal characteristics. This validation confirms that the HS model provides sufficiently accurate results for the range of Knudsen numbers considered. For this reason, more complex molecular models, such as the Variable Soft Sphere (VSS) model, were not employed in the present analysis. Four boundary types are considered—periodic, specular reflection, diffuse reflection at a fixed wall temperature, and adiabatic walls—to assess how boundary interactions influence gas dynamics and acoustic wave characteristics under rarefied conditions.

Given the wide range of applications—including MEMS/NEMS devices, vacuum electronics, gas centrifuges, and spacecraft re-entry simulations—a detailed understanding of how boundary conditions influence rarefied gas flow is essential for both theoretical studies and practical engineering designs.

2 FORMULATION OF THE PROBLEM

We considered rarefied monatomic gas between two coaxial stationary cylinders, confined between two planes perpendicular to the axis of symmetry z (two dimensional axis-symmetrical problem) with a constant walls temperature, as the temperature profile of the wall of the inner cylinder is stepwise and the conditions on plane boundaries are diffuse, adiabatic, periodic or symmetric (Fig. 1).

Depending on the boundary conditions, the flow can be considered as in a container or part of the flow between two infinite cylinders. A sudden change in inner cylinder temperature in the fluid confined between two stationary coaxial cylinders can induce the generation of acoustic waves. When a rapid thermal perturbation is applied, it causes the fluid near the heated surface to undergo instantaneous thermal expansion. This localized volumetric change results in the formation of transient pressure gradients within the fluid. Due to the compressible nature of the medium, these pressure disturbances propagate as acoustic waves. The propagation characteristics of the resulting acoustic waves are governed by the thermophysical properties of the fluid and the geometry of the domain and can be of interest in studies of heat transfer, acoustic diagnostics, and compressible fluid dynamics. Our studies commence at the moment of the sudden temperature change, which serves as the initial condition for investigating the thermoacoustic response of the fluid.

The following notations are used to describe the rarefied gas flow: ρ is the density, T is the temperature, P is the thermodynamic pressure, (u, v, w) are the velocity components in (r, ϕ, z) directions, R_1 and R_2 are the radii, and $T_1(z)$ and $T_2(z)$ are the temperatures of the inner and outer cylinders respectively (Fig. 1).

2.1 DIRECT SIMULATION MONTE CARLO METHOD

In the present study, the problem is formulated as two-dimensional and axisymmetric in physical space (r - z coordinates), while the molecular velocity distribution function remains three-dimensional. This is a standard DSMC modeling approach for cylindrical geometries with rotational symmetry. Although the spatial dependence on the azimuthal coordinate φ is neglected, all three components of molecular velocity are retained in the simulation. This ensures that momentum and energy exchanges are computed correctly, preserving the full three-dimensional character of particle motion while reducing computational cost.

The gas considered is simulated as a stochastic system of N particles [13, 14]. The macrocharacteristics are normalized by using the following scales: for density $\rho_0 = mn_0$ (m is the molecular mass, n_0 is the average number density); for velocity $V_0 = \sqrt{2RT_0}$ (R is the gas constant); for length – the distance between the cylinders $L = R_2 - R_1$; for time $t_0 = L/V_0$; for temperature T_0 – the wall temperature of the outer cylinder, which is a constant and does not depend on z . The Knudsen number is $\text{Kn} = l_0/L$, where the mean free path is l_0 . All quantities used are non-dimensional so that the mean free path at equilibrium is equal to 1.

We denote the particle velocity before collision with the wall with $(\xi_z, \xi_r, \xi_\varphi)$ and after with $(\xi_z^*, \xi_r^*, \xi_\varphi^*)$, respectively, the velocity magnitude with $c = \sqrt{\xi_z^2 + \xi_r^2 + \xi_\varphi^2}$ and $c^* = \sqrt{\xi_z^{*2} + \xi_r^{*2} + \xi_\varphi^{*2}}$, the position (r, z) and (r^*, z^*) respectively.

The basic steps of simulation are as follows:

A. The time interval $[0; \hat{t}]$ over which the solution is found is subdivided into subintervals with step Δt .

B. The space domain is subdivided into cells with sides $\Delta z, \Delta r$.

C. Gas molecules are simulated in gap G using a stochastic system of N points (particles), having position $x_i(t), r_i(t)$ and velocities $(\xi_z^i(t), \xi_r^i(t), \xi_\varphi^i(t))$.

D. N_m particles are located in the m -th cell at any given time. This number varies during the computer simulation by the following two stages:

Stage 1. Binary collisions in each cell are calculated, whereas particles do not move. Collision modeling is realized using Bird's scheme "no time counter" [13], which follows the next steps:

- Determine the Number of Collisions: $N_c = \frac{N_m(N_m - 1)\sigma_T g_{\max}\Delta t}{2V}$, where σ_T – maximum collision cross section, g_{\max} – maximum relative speed in the cell, V – cell volume;
- Select random N_c particle pairs;
- Accept the collision with probability $P = g/g_{\max}$ where $g = |\vec{\xi}_1 - \vec{\xi}_2|$ – relative speed;
- If a collision occurs, update the particle velocities using hard-sphere model collision dynamics. Let $\vec{g} = \vec{\xi}_1 - \vec{\xi}_2$ and \vec{s} be random unit vector and $\vec{g}^* = |\vec{g}| \cdot \vec{s}$. Calculate the mass center velocity $\vec{\xi}_0 = \frac{1}{2}(\vec{\xi}_1 + \vec{\xi}_2)$ and then the new post-collision particle velocity $\vec{\xi}_1^* = \vec{\xi}_0 - \frac{1}{2}\vec{g}^*$ and $\vec{\xi}_2^* = \vec{\xi}_0 + \frac{1}{2}\vec{g}^*$.

Stage 2. Particles move with new initial velocities acquired after collisions and no external forces act on particles. No collisions are accounted for at this stage.

E. Stage 1 and Stage 2 are repeated until $t = \hat{t}$.

F. Flow macro-characteristics are calculated as time-averaged as follows:

- the density $\rho = \frac{1}{N_{\text{avg}}} \sum_{k=1}^{N_{\text{avg}}} \frac{N_m^k m}{V_{\text{cell}}}$;

- the velocity $\vec{v} = \frac{1}{N_{\text{avg}}} \sum_{k=1}^{N_{\text{avg}}} \sum_{i=1}^{N_m^k} \vec{\xi}_i^k$;
- temperature $T = \frac{m}{2} \frac{1}{3k_B} \left(\frac{1}{N_{\text{avg}}} \sum_{k=1}^{N_{\text{avg}}} \sum_{i=1}^{N_m^k} \vec{\xi}_i^k \cdot \vec{\xi}_i^k - \vec{v} \cdot \vec{v} \right)$;

where k_B – Boltzmann constant, N_{avg} – number of time steps for averaging, m – molecular mass and V_{cell} – cell volume.

2.2 BOUNDARY CONDITION

We consider the boundary conditions on both plane boundaries.

Let α and β are random angles in interval $\alpha \in [0, \pi/2]$, $\beta \in [0, 2\pi]$. Using this angles are modeled randomly unit vector from the unit semi-sphere.

(A) Diffuse Boundary Condition. Gas molecules striking the wall are re-emitted in random directions according to a Maxwellian distribution, fully accommodating to the wall's temperature and velocity. This condition realistically models both thermal and momentum accommodation, assuming the wall is rough or highly interactive. It leads to velocity slip and thermal transpiration effects in the slip and transition regimes. When a gas molecule collides with the wall, it loses all memory of its incoming direction and energy, fully equilibrating with the wall before reflection. This represents a high-friction, high-interaction surface.

$$\xi_z^* = \begin{cases} \sqrt{\frac{2k_B T(r)}{m}} \cos \alpha, & z = 0 \\ -\sqrt{\frac{2k_B T(r)}{m}} \cos \alpha, & z = L_G \end{cases}$$

$$\xi_r^* = \sqrt{\frac{2k_B T(r)}{m}} \sin \alpha \cos \beta$$

$$\xi_\varphi^* = \sqrt{\frac{2k_B T(r)}{m}} \sin \alpha \sin \beta$$

$$T(r) = \frac{r - R_1}{R_2 - R_1} (T_2 - T_1(z)), \quad z = 0 \text{ and } z = L_G$$

$$r^* = r$$

$$z^* = z$$

The linear temperature distribution at $z = 0$ and $z = L_G$ is used.

(B) Adiabatic Boundary Condition. No heat transfers across the plane boundary wall – ensures thermal insulation; often paired with diffuse reflection in simulations. No heat is exchanged between the wall and the gas. The normal component of heat flux across the boundary surface is zero. The gas temperature near the wall can change, but the wall itself does not supply or absorb heat. It models a thermally insulated wall. This gas-surface interaction model can be described by keeping the particle velocity magnitude invariant and the velocity direction of the reflected particle set based on isotropic scattering boundary conditions in the half unit sphere.

$$\begin{aligned}\xi_z^* &= c \cos \alpha \\ \xi_r^* &= c \sin \alpha \cos \beta \\ \xi_\varphi^* &= c \sin \alpha \sin \beta \\ r^* &= r \\ z^* &= z\end{aligned}$$

The difference between diffusion and adiabatic reflection is only the coefficient. At the diffusion reflection the coefficient $\sqrt{2k_B T_1/m}$ depends on the wall temperature and the particle mass while at the adiabatic reflection the coefficient c is the particle velocity magnitude before collision on the particle with the wall.

(C) Symmetric Boundary Condition. Assumes symmetry across planes $z = 0$ and $z = L_G$ (Fig. 1), meaning no normal flow or shear stress. Reduces the domain size by taking advantage of flow symmetry. Often applied at the mid-plane of a vortex pair or for simplified simulation domains. A plane of mirror symmetry: no flow perpendicular to the boundary, no shear stress across it, and no temperature gradient across it. Represents half or a portion of a symmetric flow field. It's not a physical wall but a computational simplification used when the flow is known to be symmetric.

$$\begin{aligned}\xi_z^* &= -\xi_z \\ \xi_r^* &= \xi_r \\ \xi_\varphi^* &= \xi_\varphi \\ r^* &= r \\ z^* &= z\end{aligned}$$

(D) Periodic Boundary Condition. Flow exiting one end of the domain re-enters at the other. Common in idealized simulations of infinite or repeating domains (e.g., axial direction of an infinitely long Taylor-Couette system). Neglects end-wall effects; ideal for isolating core flow behavior without boundary disturbances. What

leaves one boundary of the domain enters at the opposite side with the same properties. There is no net change across the boundary. Models repeating geometries or infinitely long domains, allowing simulations to neglect end-wall effects and focus on the fully developed flow region.

$$\begin{aligned}\xi_z^* &= \xi_z \\ \xi_r^* &= \xi_r \\ \xi_\varphi^* &= \xi_\varphi \\ r^* &= r \\ z^* &= \begin{cases} L_G - z, & z = 0 \\ z - L_G, & z = L_G \end{cases}\end{aligned}$$

3 NUMERICAL RESULTS

We study the influence of boundary conditions on the thermoacoustic waves in the rarefied gas between two stationary cylinders. The waves are generated by the inner cylinder temperature shock change (with 100% on the one half) compared to the initial one. The studied cases are in for variants for the axial boundary conditions – diffuse, adiabatic, symmetric and periodic. The studied boundary conditions may be important in the case of a system with different temperature control of the plain boundary conditions. Based on the Navier-Stokes-Fourier (NSF) model and Direct Simulation Monte Carlo (DSMC) method developed in previous publications and their numerical solutions [10, 11], are considered transient processes in the gas phase.

In numerical calculation are used the Knudsen number $\text{Kn} = 0.02$, the initial temperature of the cylinders $T_0 = 1$, the inner cylinder radius $R_1 = 1$, the outer cylinder radius $R_2 = 2$, the distance between cylinders $L = R_2 - R_1 = 1$, cylinders length $L_G = 2L = 2$, the inner cylinder temperature $T_1(z) = \begin{cases} 2T_0, & 0 \leq z < L \\ T_0, & L \leq z \leq 2L \end{cases}$ and the outer cylinder temperature $T_2 = T_0$. The two cylinders are stationary. We use the four kinds of axial boundary conditions for the planes $z = 0$ and $z = L_G$, and the diffuse at the cylinders.

To assess whether the calculated flow field exhibits genuine three dimensional behavior or can be approximated as two dimensional (axisymmetric), we performed an azimuthal (φ) averaging of macroscopic quantities and quantified their φ -dependent fluctuations. For each spatial location (x, r) , the time averaged field $\langle Q \rangle_\varphi$ was computed, and the root mean square (RMS) deviation with respect to φ was ob-

Table 1. Normalized azimuthal fluctuation metric for density, temperature, and velocity components under diffuse, adiabatic, symmetric and periodic transverse boundary conditions

	Density	Temperature	Velocity		
	ρ_φ	T_φ	axial $v_{1\varphi}$	radial $v_{2\varphi}$	azimuthal $v_{3\varphi}$
diffuse	5.829×10^{-5}	9.336×10^{-6}	4.711×10^{-2}	9.058×10^{-2}	1.365
adiabatic	1.339×10^{-5}	9.863×10^{-6}	1.183×10^{-1}	8.725×10^{-2}	1.514
symmetric	1.340×10^{-5}	9.708×10^{-6}	1.065×10^{-1}	8.801×10^{-2}	1.333
periodic	1.318×10^{-5}	9.736×10^{-6}	1.021×10^{-1}	1.100×10^{-1}	1.216

tained [13–15]. A normalized measure of φ -dependence,

$$\rho_\varphi = \frac{\sum_{x,r} \text{std}[\langle \rho \rangle_\varphi]^2}{\sum_{x,r} \langle \rho \rangle_\varphi^2} \quad \text{for density,}$$

$$T_\varphi = \frac{\sum_{x,r} \text{std}[\langle T \rangle_\varphi]^2}{\sum_{x,r} \langle T \rangle_\varphi^2} \quad \text{for temperature,}$$

$$v_{i\varphi} = \frac{\sum_{x,r} \text{std}[\langle v_i \rangle_\varphi]^2}{\sum_{x,r} \langle v_i \rangle_\varphi^2} \quad \text{for axial, radial and azimuthal velocity components.}$$

For all cases considered (diffuse, adiabatic, symmetric, and periodic), the values E_Φ for density and temperature are uniformly small (Table 1). These values indicate that the azimuthal variation of the primary thermodynamic fields is negligible compared to their mean magnitude, demonstrating a high degree of statistical axisymmetry. The axial and radial velocity components exhibit moderate E_Φ values, ranging from $O(10^{-2})$ to $O(10^{-1})$. While larger than those of density and temperature, these values remain small in absolute terms and do not indicate the presence of coherent azimuthal flow structures. Instead, they reflect weak azimuthal variability that is consistent with finite-sampling statistical noise inherent to particle-based simulations. By contrast, the azimuthal velocity component yields comparatively large E_Φ values for all boundary conditions. This behavior is expected and does not contradict the assumption of axisymmetry. The mean azimuthal velocity is approximately zero throughout the domain; consequently, the normalization in the definition of E_Φ amplifies fluctuations arising from statistical noise. These fluctuations represent random deviations about a zero mean rather than a persistent φ -dependent flow component. Taken together, the results demonstrate that the macroscopic structure

of the flow is effectively independent of the azimuthal coordinate. The negligible φ -dependence of density and temperature, combined with the absence of systematic azimuthal velocity components, indicates that the flow can be accurately described as two-dimensional (axisymmetric). Any residual azimuthal variability is attributable to statistical uncertainty rather than genuine three-dimensional dynamics.

Flow modeling in the present study is conceptually divided into two distinct stages: (1) the transient regime, during which the system evolves dynamically in response to the initial thermal disturbance (Figs. 2–4); and (2) the steady-state regime, wherein the flow variables stabilize and no longer exhibit significant time variation (Figs. 5–7).

The transient regime (1). Figure 2 illustrates the temporal variation of the temperature T at two spatial locations within the gas domain: a point ($x = 0.02$, $r = 1.42$) proximate to the plane $z = 0$ and a point ($x = 0.52$, $r = 1.42$) in the middle of the gas gap. These results capture the propagation of thermoacoustic waves triggered by the localized temperature shock. The temperature evolution reflects both the initial thermal pulse and its subsequent dissipation or reflection, contingent upon the axial boundary condition. Differences in waveform characteristics—such as amplitude, frequency, and damping behavior—highlight the significant role boundary conditions play in governing thermal transport and wave reflection in confined rarefied media. Figure 3 presents the time-dependent behavior of the gas density ρ at the same spatial points as in Fig. 2. The variations in density arise due to pressure fluctuations accompanying the thermal wave. These results elucidate the compressibility effects within the rarefied medium and reveal how axial boundary conditions influence mass trans-

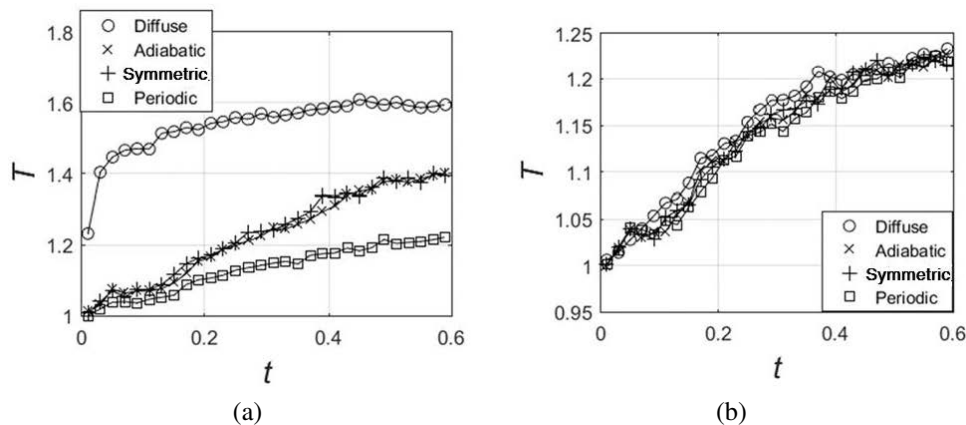


Fig. 2. The temperature T variation at the time at point: (a) $z = 0.02$, $r = 1.42$; (b) $z = 0.52$, $r = 1.42$.

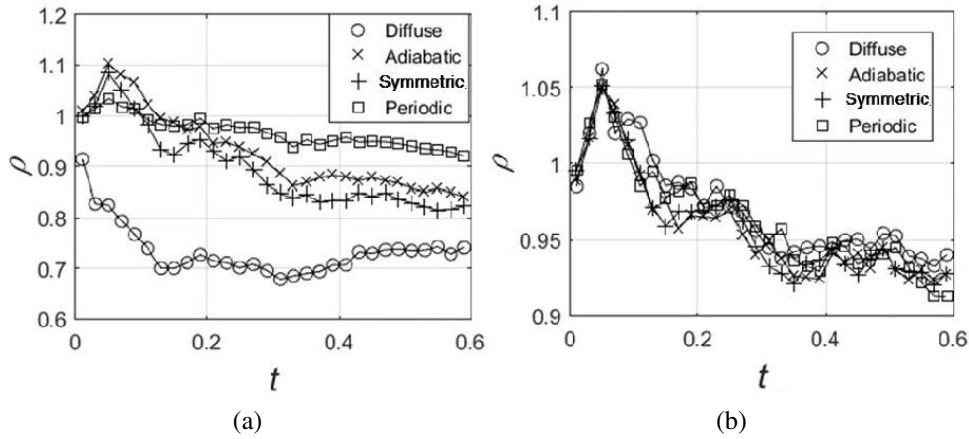


Fig. 3. The density ρ variation at the time at point: (a) $z = 0.02, r = 1.42$; (b) $z = 0.52, r = 1.42$.

port and wave propagation dynamics. Figure 4 depicts the radial component of the gas velocity v at the same two positions. These profiles provide insight into the induced flow field resulting from the temperature discontinuity. The observed velocity oscillations are indicative of thermoacoustic wave propagation and are affected by the extent to which axial boundaries permit or restrict wave motion. The analysis of radial velocity is particularly relevant for evaluating momentum transport mechanisms and flow symmetry under different boundary configurations. Together, Figs. 2–4 offer a comprehensive view of the transient thermal, density, and velocity fields that

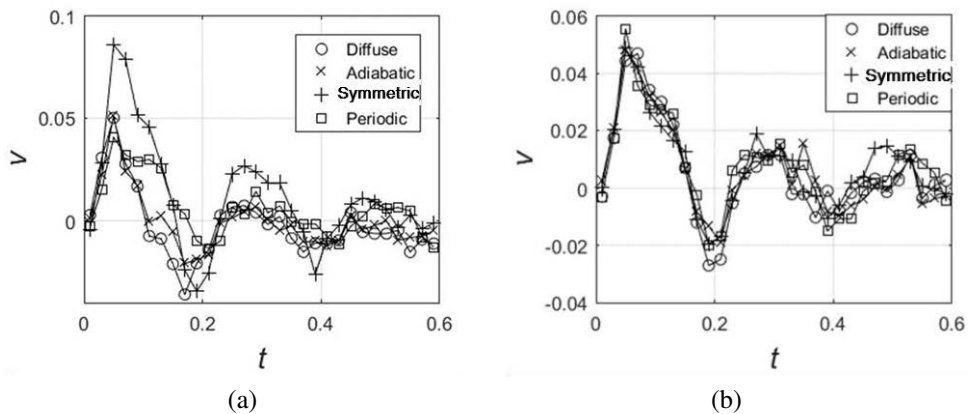


Fig. 4. The radial velocity v variation at the time at point: (a) $z = 0.02, r = 1.42$; (b) $z = 0.52, r = 1.42$.

develop in response to an impulsive thermal disturbance in a rarefied cylindrical gas system. The findings underscore the critical importance of axial boundary conditions in shaping the wave characteristics and energy dissipation behavior in thermoacoustic processes. These results contribute to a deeper understanding of nonequilibrium gas dynamics in micro- and mesoscale systems where rarefaction effects are non-negligible.

The steady-state regime (2). Figure 5 depicts the steady-state temperature distribution along the axial direction (z -axis) of the gas phase for various axial boundary conditions imposed on the end surfaces of the cylindrical domain. The temperature profiles are presented for four fixed radial positions: $r = 1.02$, $r = 1.3$, $r = 1.62$ and $r = 1.98$. In proximity to the inner cylinder wall ($r = 1.02$), the discrepancies

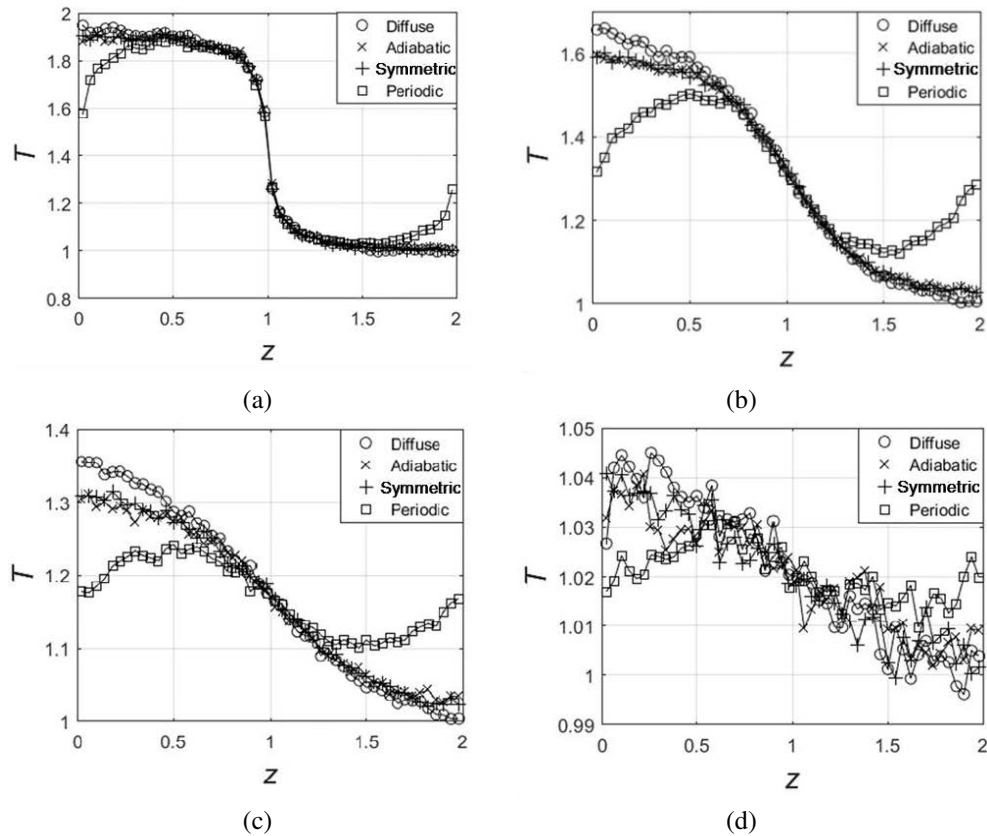


Fig. 5. The temperature variation T at time 3.01: (a) $r = 1.02$; (b) $r = 1.3$; (c) $r = 1.62$; (d) $r = 1.98$.

among the temperature profiles corresponding to the different boundary conditions are relatively minor. This can be attributed to the strong thermal influence of the inner cylinder's surface temperature, which dominates in this region. However, as the radial distance from the inner cylinder increases – particularly at $r = 1.3$ and $r = 1.62$ —the impact of the boundary conditions becomes more pronounced. In these regions, the effects of adiabatic boundaries are especially evident, as they restrict heat exchange at the axial ends, thereby modifying the overall temperature gradient within the domain. The enhanced sensitivity at these mid-gap radial positions results from the dynamic behavior of the rarefied gas responding to the imposed temperature gradient. At the outer radial position ($r = 1.98$), near the outer cylinder wall, the temperature profiles exhibit irregularities or non-monotonic behavior. Although the magnitude of temperature fluctuations remains relatively small, the loss

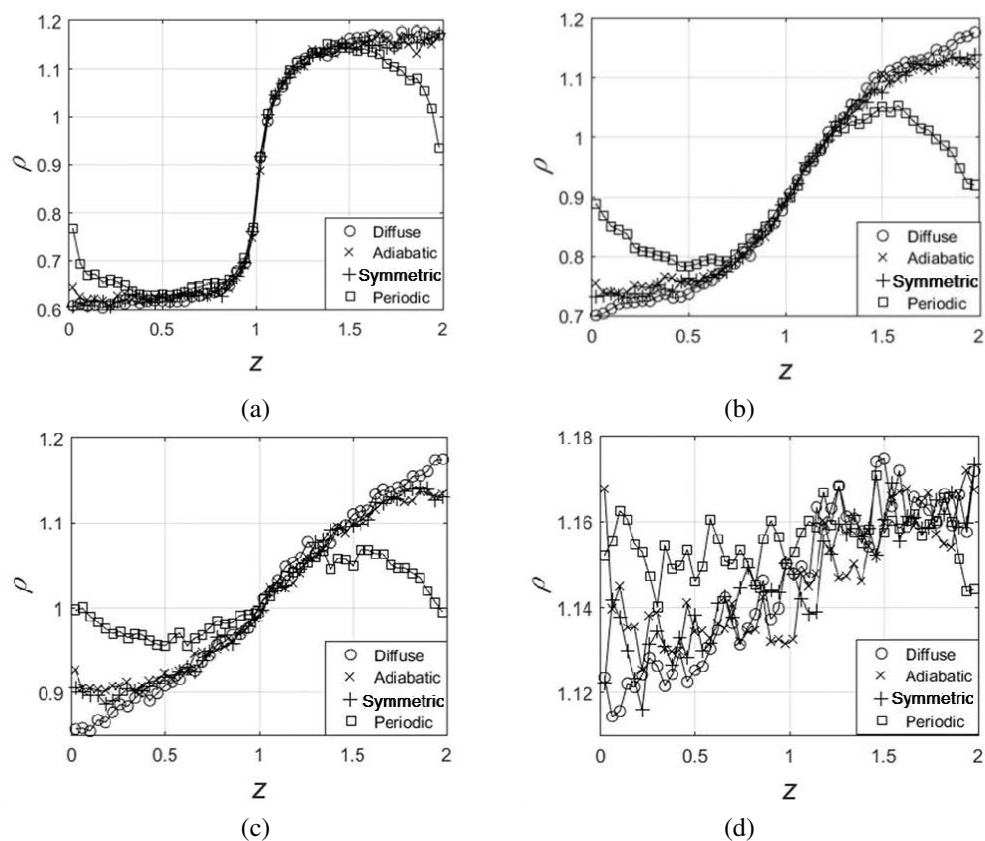


Fig. 6. The density ρ variation at time 3.01: (a) $r = 1.02$; (b) $r = 1.3$; (c) $r = 1.62$; (d) $r = 1.98$.

of smoothness in the profiles suggests the presence of localized disturbances or weak instabilities, potentially arising from the combined effects of geometric confinement and rarefaction. A similar trend is observed in the corresponding density distributions shown in Fig. 6. The density variations under different boundary conditions display greater sensitivity compared to the temperature fields. This enhanced variability is attributed to the coupling between density and the axial velocity field. Specifically, Fig. 7 illustrates the axial velocity component u near the inner and the gaps middle, respectively. Fluctuations in axial velocity, particularly under rarefied gas conditions, induce additional perturbations in the density distribution. These interactions lead to amplified deviations and local fluctuations in density, particularly near the boundaries, underscoring the complex interplay between thermal gradients, gas motion, and boundary effects in no equilibrium regimes.

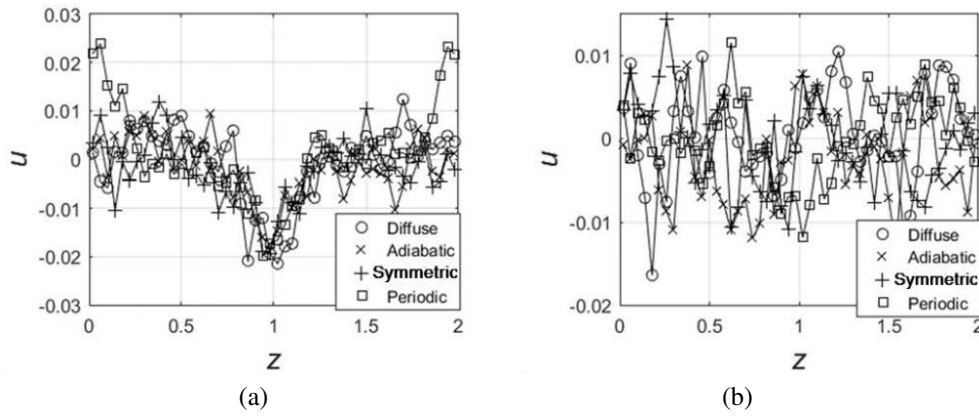


Fig. 7. The axial velocity u variation at time 3.01: (a) $r = 1.02$; (b) $r = 1.3$.

4 CONCLUSIONS

Flow evolution was characterized in two stages: a transient regime, where thermoacoustic waves propagate and reflect depending on boundary type, and a steady-state regime, where temperature, density, and velocity distributions stabilize. Results show that axial boundary conditions significantly influence wave dynamics, energy dissipation, and flow structure, particularly at greater radial distances from the inner cylinder. These findings highlight the importance of boundary modeling in rarefied gas systems and provide insights relevant to microscale thermal management and gas dynamics.

REFERENCES

- [1] SHINGO KOSUGE (2015) Cylindrical Couette flow of a rarefied gas: Effect of a boundary condition on the inverted velocity profile. *Physical Review E* **92** 013013.
- [2] N.T.P. LE, N.A. VU, L.T. LOC, T.N. THOAI (2017) New temperature jump boundary condition in high-speed rarefied gas flow simulations. *Vietnam Journal of Mechanics* **39**(2) 165–176.
- [3] D.A. LOCKERBY, J.M. REESE, D.R. EMERSON, R.W. BARBER (2004) Velocity boundary condition at solid walls in rarefied gas calculations. *Physical Review E* **70** 017303.
- [4] T. MISSONI, H. YAMAGUCHI, I. GRAUR, S. LORENZANI (2021) Extraction of Tangential Momentum and Normal Energy Accommodation Coefficients by Comparing Variational Solutions of the Boltzmann Equation with Experiments on Thermal Creep Gas Flow in Microchannels. *Fluids* **6**(12) 445.
- [5] G. TATSIOS, A. TSIMPOUKIS, D. VALOUGEORGIS (2021) The Half-Range Moment Method in Harmonically Oscillating Rarefied Gas Flows. *Fluids* **6**(1) 17.
- [6] A.A. FROLOVA (2021) Analysis of the Boundary Conditions for Rarefied Molecular Gases with Partial Accommodation Coefficients and Energy Exchange. *Computational Mathematics and Mathematical Physics* **61** 1672-1681.
- [7] P. TZENG, W. CHOU, C. LIU, W. LI (2011) Improvement of the Gas-Surface Collision Rule for Adiabatic Walls in DSMC Modeling of Rarefied Gas Convection in a Micro Enclosure. *Journal of Aeronautics, Astronautics and Aviation, Series A* **43**(3) 147-158.
- [8] A. MOHAMMADZADEH, A. RANA, H. STRUCHTRUP (2016) DSMC and R13 modeling of the adiabatic surface. *International Journal of Thermal Sciences* **101** 9-23.
- [9] V. KOSYANCHUK (2024) Numerical study of microscale gas pump based on surface acoustic waves. *Physics of Fluids* **36**(3) 032012.
- [10] P. GOSPODINOV, D. DANKOV, V. ROUSSINOV, M. MIRONOVA (2022) Acoustic waves modeling Taylor-Couette flow in rarefied gas at inhomogeneous cylinder wall temperature distribution. *AIP Conference Proceedings* **2522** 080001.
- [11] P. GOSPODINOV, D. DANKOV, V. ROUSSINOV, M. MIRONOVA (2017) Numerical simulation of the pulsed Pirani gauges. *AIP Conference Proceedings* **1895** 080003.
- [12] D. DANKOV, M. MIRONOVA, P. GOSPODINOV (2025) Acoustic waves modeling flow in rarefied gas between stationary cylinders at oscillation inhomogeneous inner cylinder wall temperature. *Journal of Theoretical and Applied Mechanics, Sofia* **55** 133-146.
- [13] G.A. BIRD (1994) “Molecular Gas Dynamics and the Direct Simulation of Gas Flows”. Oxford University Press, Oxford.
- [14] C. CERCIGNANI (2000) “Rarefied Gas Dynamics, From Basic Concepts to Actual Calculations”. Cambridge University Press, Cambridge.
- [15] A. GARCIA, W. WAGNER (2000) Time step truncation error in direct simulation Monte Carlo. *Physics of Fluids* **12** 2621-2633.